Journal of Materials Chemistry C

Accepted Manuscript

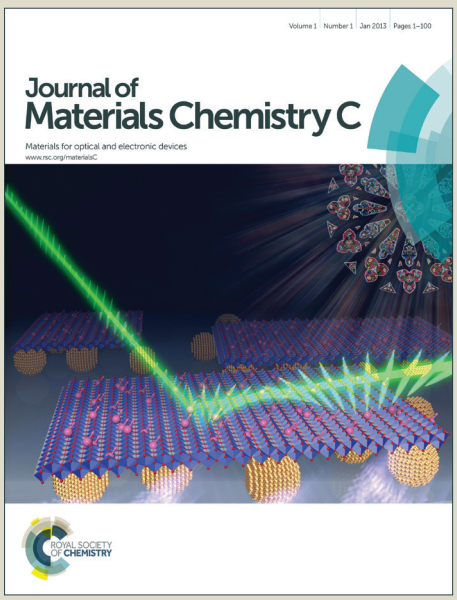

ROYAL SOCIETY OF CHEMISTRY

www.rsc.org/materialsC

Journal of Materials Chemistry C

Dynamic Article Links ►

Cite this: DOI: 10.1039/c0xx00000x

ARTICLE TYPE

www.rsc.org/xxxxxx

Study of the influences of molecular planarity and aluminium evaporation rate on the performances of electrical memory devices

Hongzhang Liu,[a] Rongcheng Bo,[a] Haifeng Liu,[a] Najun Li,[a] Qingfeng Xu,[a] Hua Li*[a], Jianmei Lu*[ab] and Lihua Wang[a]

Received (in XXX, XXX) Xth XXXXXXXXX 20XX, Accepted Xth XXXXXXXXX 20XX
DOI: 10.1039/b000000x

In this paper, two conjugated small molecules (**CZ-BT** and **TPA-BT**) were designed and successfully synthesized to investigate the influence of different electron donor moieties on thin-film morphology and their electrical memory devices properties. Current-voltage (I-V) curves indicated that both **CZ-BT** and **TPA-BT** exhibited stable dynamic random access memory (DRAM) characteristics under appropriate Al evaporation rate condition, but with different threshold voltages, former was lower than later due to its better film morphology and closer intermolecular stacking. Furthermore, the performances of the two devices under different Al electrode evaporation rate were also investigated and the results showed that the **CZ-BT** based device still exhibited original DRAM characteristic while the **TPA-BT** based device exhibited WORM characteristic when the Al electrode evaporation rate was increased to 5 Å/s. The variation of storage characteristics of **TPA-BT** could be mainly attributed to its poor film-forming property and the Al nano-particles would penetrate into the film during the quickly evaporation process to form filamentary conduction leading to WORM behaviour.

Introduction

Microelectronics technology based on small organic molecules and polymers have attracted increasing interest due to their many advantages, such as low cost, large scalability, structure designable.[1-15] Especially, the above mentioned materials have potential to be fabricated as high density data-storage devices compared with the traditional silicon based devices for their 3D-stack ability, which could greatly improve the number of memory cells in unit volume.[1, 3, 16-20] The Kang,[21] Ree[22-24] and Chen[23, 25-27] groups have spent a lot of energies on studying the relationship between the molecular structure and the device storage type. For example, they have achieved different memory types such as WORM, Flash, SRAM and DRAM devices through adjustment of strength and weakness of electron donors and acceptors. Our group has been engaging in tuning memory device characteristics through change molecular conjugated length,[28] soft-alkyl chain length[29-30] and molecular planarity.[31] However, the stability of electric memory device performance is yet a vital topic. There are so many factors which would do effect on device performance still remained unknown, such as the film surface roughness,[32] the film thickness[33-36] and the molecular or electrode deposition rate,[37] etc.

Carbazole (CZ) and triphenylamine (TPA) are well known electron donors and often used as the donor fragments of hole transporting material.[32, 38-40] Compared with the other electron donors, triphenylamine compounds can form ammonium ion radicals in the electric field, leading to a good hole transport property. Generally, such compounds have a suitable glass transition temperature, excellent thermal stability and chemical stability, these properties make sure the long-term and stable device. On the other hand, carbazole is also a well-known electron donor and widely used as high thermal stability of the hole transport material due to its special rigid structure and a variety of functional modifications in 3, 6, 9 positions of its molecular backbone.[41] In this paper, we synthesized two molecules which containing TPA and CZ moieties (**CZ-BT** and **TPA-BT**) as shown in Scheme 1.

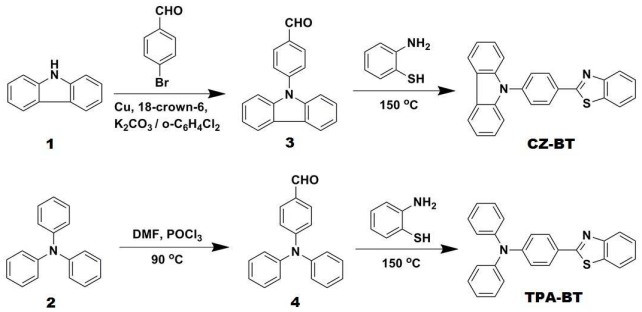

Scheme 1. Chemical structures and synthesis routes of two small molecules.

According to the results revealed by AFM and XRD, **CZ-BT** has a better film-forming property, with RMS of about 2 nm than that of **TPA-BT** with RMS of about 10 nm. *I-V* characteristics indicated that both molecules based devices exhibited stable DRAM characteristics and the switching threshold of **CZ-BT** is

lower than **TPA-BT**. This is due to **CZ-BT**'s better planarity and lead to a closer intermolecular π-π stacking. Furthermore, the influence of different evaporation rate of aluminum electrode was investigated and found that when the evaporation rate of aluminum was increased to 5 Å/s, the **TPA-BT** based device showed WORM characteristic compared to its original DRAM characteristic as the evaporation rate of aluminum was about 0.5 Å/s. However, the memory behavior of **CZ-BT** based device had nothing to do with the electrode evaporation rate. We hope the concluded influences of molecular planarity and electrode evaporation rate on the device performance could offer a guidance in the future materials design and synthesis.

Results and discussion

Thermal properties of **CZ-BT** and **TPA-BT** were investigated by TGA (Fig. S1, Supporting Information). All of the compounds exhibit good thermal stability with thermal decomposition temperatures (5% weight loss temperature) of 294 °C (**CZ-BT**) and 272 °C (**TPA-BT**), respectively. It indicates that the materials can endure heat deterioration in the memory devices and have a relatively wide range for practice.

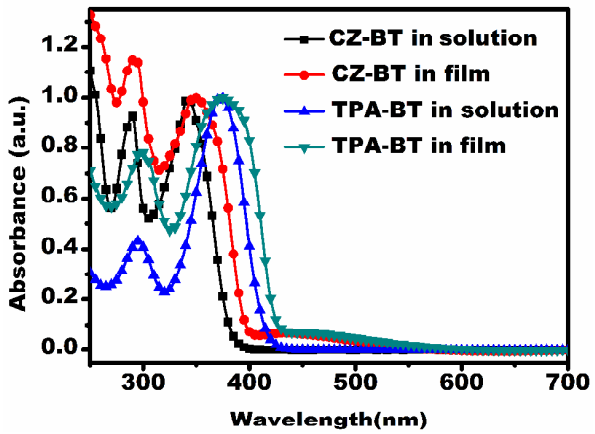

Fig. 1 UV-Vis absorption spectra of the two compounds in CH_2Cl_2 solution and solid thin films on a quartz substrate.

As shown in Fig. 1, the UV-Vis absorption spectrum of **CZ-BT** in dilute dichloromethane solution exhibits a absorption peak at 291 nm, which is attributed to the n-π* transition of the carbazole moiety, and a stronger absorption peak at 341 nm due to the π-π* transition of the aromatic groups of the carbazole moiety. And the UV-vis spectra of **TPA-BT** in solution also generates two absorption peaks (295 nm and 375 nm), and the generation mechanism is similar to the former.[42-44] We also measured the UV-Vis absorption spectrum of the vacuum-deposited thin films of **CZ-BT** and **TPA-BT**. Compared with the absorption spectrum in solution state, both absorption peaks in the film state happened a red-shift (from 341 nm to 352 nm in **CZ-BT** film) or significantly broadened (in **TPA-BT** film), indicating that they stacked orderly and closely during the molecule deposition state,[45] which is coincidence with the results revealed by AFM and XRD.

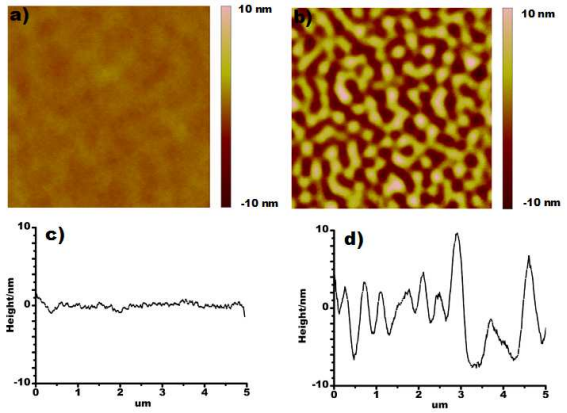

Fig. 2 Tapping-mode height and a typical cross section profile of AFM topographic images of compounds thin film vacuum-deposited onto ITO at room temperature: **CZ-BT** (a, c); **TPA-BT** (b, d).

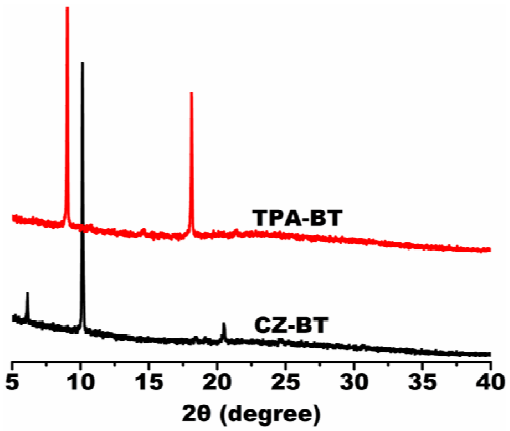

Fig. 3 X-ray diffraction spectra of **CZ-BT** and **TPA-BT** films deposited on ITO glass substrates.

Fig. 2 shows the film surface morphology of the both two compounds. The tapping-mode AFM phase image of the **CZ-BT** film exhibits a smooth, featureless morphology as shown in Fig. 2a, the root-mean-square (RMS) roughness does not exceed 5 nm (Fig. 2c). This type of flat and featureless morphology of the film facilitates the charge injection from the electrode into the organic molecules layer.[32] Moreover, the good surface morphology can also prevent the aluminum (Al) penetrating into the organic film during the vacuum deposition of aluminum electrode. However, the regular and hilly-like morphology of the "counterpart" compound **TPA-BT** shows the rougher morphology surface and the RMS is up to 10 nm (Fig. 2b and Fig. 2d). The 3D-AFM topography images of the two compounds are shown in Fig. S2a and Fig. S2b (Supporting Information). In addition, we investigated the tapping-mode AFM phase image of the **TPA-BT** film, which is prepared by vacuum vapor deposition using a heated substrate (about 60 °C), and found the accumulation of molecules tend to be worse as shown in Fig. S3. The XRD patterns of the two compounds films deposited on ITO glasses are shown in Fig. 3. There are three diffraction peaks in **CZ-BT** film, which are located at 2θ = 6.1°, 10.2° and 20.4° (4.3 Å), indicating the **CZ-BT** molecule adopts well π-π stacking in the thin film. Furthermore, the 2θ = 10.2° (8.6 Å) is almost twice that

of 2θ = 20.4° (4.3 Å) indicating the **CZ-BT** molecule has good layer by layer stacking in the film. Similarly, in **TPA-BT** film there are two diffraction peaks at 2θ = 9.0° and 18.1° (4.9 Å), respectively. The sharp diffraction peaks and layer by layer stacking of **CZ-BT** and **TPA-BT** films illustrate that both molecules self-assembled into highly ordered crystalline film well. Meanwhile, it can be concluded that **CZ-BT** molecule packed more closely and orderly than **TPA-BT** based on the results of AFM morphology and XRD spectrum.

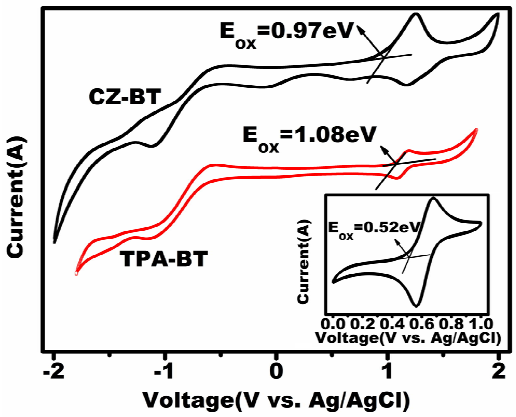

Fig. 4 Cyclic voltammetry (CV) curves of the two compounds in anhydrous dichloromethane solution with 0.1 M of N^+-$Bu_4ClO_4^-$ as the supporting electrolyte. The inset of Fig. 4 shows the CV curve of the ferrocene standard swept in the same conditions as that for the two compounds. The scan rate was 100 $mV \cdot s^{-1}$.

The band gap of **CZ-BT** between the highest occupied molecular orbital (HOMO) and the lowest unoccupied molecular orbital (LUMO) energy levels estimated from the onset of the absorption spectrum is 3.14 eV by the following equation: $E_g = hc/\lambda_{Edge}$. The electrochemical property of **CZ-BT** was measured by cyclic voltammetry-(CV) using a 0.1 M solution of tetrabutylammonium perchlorate (TBAP) in anhydrous dichloromethane, as shown in Fig. 4. The onset oxidation $E_{ox}^{(onset)}$ of **CZ-BT** is 0.97 eV. Note that the $E_{Ferrocene}$ is 0.52 eV from the CV measurement. The HOMO and LUMO energy levels were calculated by the following equation:

$$E_{HOMO} = -[E_{ox}^{(onset)} + 4.8 - E_{Ferrocene}]$$

$$E_{LUMO} = E_{HOMO} + E_g$$

where E_{HOMO} and E_{LUMO} are the HOMO and the LUMO energy levels, and $E_{ox}^{(onset)}$ is the onset oxidation potential of the molecule. $E_{Ferrocene}$ is the external standard potential of the ferrocene/ferrocenium ion couple, 4.80 is the reference energy level of ferrocene. The HOMO and LUMO values were determined to be -5.25 (or -5.36) and -2.11 (or -2.43) eV for **CZ-BT** and **TPA-BT** in DCM, respectively. The energy barrier (Φ_1) between work functions of ITO (4.8 eV) and HOMO energy level for **CZ-BT** is 0.45 eV, which is much lower than the energy barrier (Φ_2) of 2.17 eV between the work functions of Al (4.28 eV) and LUMO energy level. It indicates that hole injection from ITO into the HOMO is much easier than electron injection from Al into the LUMO level for **CZ-BT**. **TPA-BT** has the similar electrochemical properties. Therefore, both two compounds are the p-type materials, and holes injection predominate the conduction process of the memory devices.[30, 46] All of the above data is listed in Table 1.

Table 1 Optical and electrochemical properties of both compounds.

Compound	E_g (eV)	HOMO (eV)	LUMO (eV)	Φ_1 (eV)	Φ_2 (eV)
CZ-BT	3.14	-5.25	-2.11	0.45	2.17
TPA-BT	2.93	-5.36	-2.43	0.56	1.85

A schematic sandwich structure comprising of many top electrodes (Al), a layer of small organic molecules and the bottom electrode (ITO) is shown in Fig. 5a. The thickness of the electroactive organic film is about 200 nm, as measured by scanning electron microscopy (SEM). The current-voltage (I-V) characteristics of the ITO/**CZ-BT**/Al device are shown in Fig. 5b. In the first round scan from 0 to -4 V, the current increased dramatically at a threshold voltage around -1.42 V, indicating a transition from a low-conductivity state (OFF state) to a high-conductivity state (ON state). The device remained in this ON state during a subsequent scan followed by the first scan from 0 to -4 V (sweep 2). However, about one minute power off after the second scan, the current was back to the OFF state and the abrupt current increase could be observed again at switching threshold voltages around -1.46 V by the third voltage scan (sweep 3). The device remained in this ON state during an immediately subsequent scan from 0 to 4 V (sweep 4). The characteristics of the device relaxing to OFF state after power off illustrated that the device based on **CZ-BT** is dynamic random access memory (DRAM) type. Under a constant voltage of -1 V, no significant degradation was observed in the OFF and ON states for over 100 min, as shown in the inset in Fig. 5b. Furthermore, the OFF and ON states were also stable up to 10^8 write-read cycles under the effect of continuous read pulses of -1 V as shown in Fig. S4a (Supporting Information). Similar to **CZ-BT**, the device based on **TPA-BT** showed DRAM memory characteristics, too, as shown in Fig. 5c. However, the switching voltage of **TPA-BT** based device was located at about -2.0 V, which is higher than that of **CZ-BT** based device, may possibly due to the higher energy gap between the organic film and the ITO electrode. The inset in Fig. 5c and Fig. S4b (Supporting Information) exhibited that the device based on **TPA-BT** also have the long-term stability. In addition, the retention time test of the two compounds based device was measured to clarify the volatile process of the device as shown in Fig. S5. It is noteworthy that the ON/OFF current ratios of both compounds are almost up to 10^5, which lead to a low misreading rate for memory storage device applications, as well, the switching threshold voltages are all lower than -2 V, and the reading voltage is only -1 V, which indicate that the organic memory device has the high stability and low power consumption.[30, 47]

Above we have concluded that the **CZ-BT** molecular packed more closely and orderly than **TPA-BT** in the deposited film. We also explored that the current-voltage characteristics of **TPA-BT** based device under the condition of aluminum evaporation rate of 5 Å/s and found that the storage type of the device transformed into a typical nonvolatile WORM memory behavior from DRAM memory behavior as shown in Fig. 5e, mainly due to the rapid

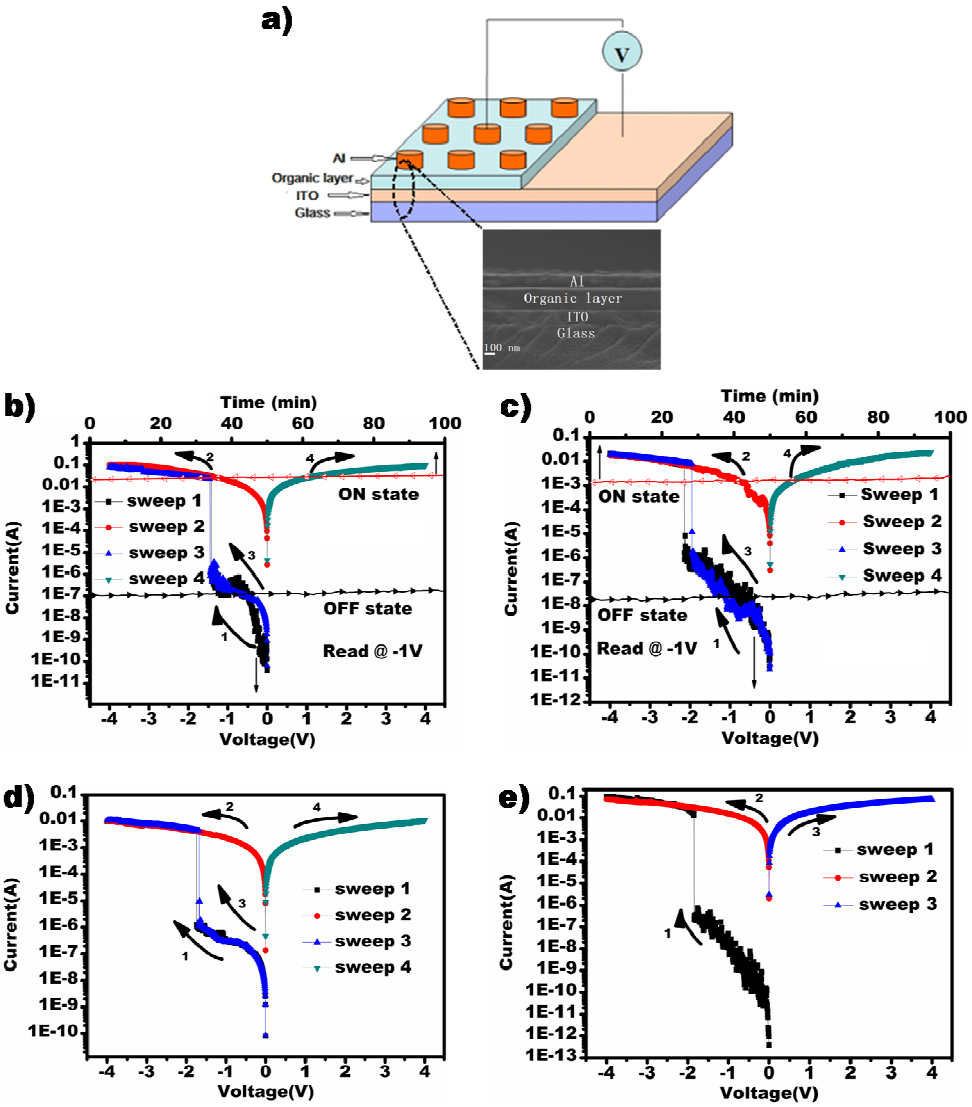

Fig. 5 (a) (top) Schematic diagram of the sandwich device; (bottom) SEM image of a cross-section view of the device; current-voltage (I-V) characteristics of the ITO/compound/Al device (The evaporation rate of aluminum is about 0.5 Å/s) and its corresponding stability in two states under a constant read voltage of -1 V, (b) **CZ-BT**, (c) **TPA-BT**; current-voltage (I-V) characteristics of the memory device fabricated with compound film (The evaporation rate of aluminum is 5 Å/s), (d) **CZ-BT**, (e) **TPA-BT**.

evaporation rate lead to the aluminum penetration, which is substantiated via investigating the cross-section EDS (Fig. S6) of the corresponding device. To further illustrate the above phenomenon we deposited a layer of LiF on the **TPA-BT** film with thickness of about 5 nm. Then aluminum electrode was evaporated onto the layer of LiF with the rate of 5 Å/s. Thus formed device exhibited original DRAM behavior as shown in Fig. S7. In addition, we used metal Ag instead of the Al top electrode to demonstrate related metal filamentary mechanism, the I-V curves are presented in Fig. S8. On the other hand, the **CZ-BT** based device still exhibited initial DRAM behavior when the evaporation rate of the aluminum electrode is 5 Å/s as shown in Fig. 5d. In addition, we found that the switching threshold voltage (about -1.5 V) of device based on **CZ-BT** is lower than **TPA-BT**, it indicates that the memory storage device based on **CZ-BT** can transmit charge easier, which was related with the conclusion above well.

To better understand the switching behavior of the devices based on the two compounds, the electronic properties of **CZ-BT** and **TPA-BT** were explored through density functional theory with the Gaussian 03 program. The HOMO, LUMO and LUMO+1 surfaces for the two molecules are shown in Fig. 6. Both the HOMO and LUMO+1 tend to locate on the donor side (CZ, TPA), while the LUMO locate on the acceptor (BT) and form the distinct asymmetric distribution. Some electrons at the HOMO may overcome the band gap via accumulating energy, then transiting to the LUMO+1 resulting in an excited state. On the other hand, electrons at the HOMO could also be excited to LUMO with a lower energy barrier. So it implies that CT

can occur to form conductive channel through the process either from the LUMO+1 of donor to the LUMO of acceptor or from the HOMO of donor to the LUMO of acceptor.[9, 47, 48] It indicates that the excitation of the donor units (CZ, TPA) leads to the intra or intermolecular CT state. With the interaction between molecules in film, the open pathway will be formed by the increasing of the migrating carriers. Thus, the device can switch from the OFF state to the ON state. When the power is turned off, the charge recombination through the D-A connection due to the unstable CT state and the memory device rapidly return to the original OFF state in a very short time. Therefore, the unstable CT states lead to the DRAM behavior. Besides, the calculated dipole moment of **CZ-BT** is only 1.197 D and 1.913 D for **TPA-BT**, indicating that the polarities of the two compounds are not strong enough to retain the charge transfer state and thus accounting for the short retention time of the ON state.[44, 47] In addition, orderly and close molecular packing in the film of **CZ-BT** can facilitate the formation of the free carrier transport pathways and reduce the charge carrier injection barrier from the ITO to the **CZ-BT** layer (Fig. 6c).[49] It means that the storage cell of device based on **CZ-BT** switches from OFF state to ON state under a relatively low voltage bias. In contrast, the storage cell of device based on **TPA-BT** needs a higher turn-on voltage to reach ON state because of its relatively poor intermolecular packing. When the evaporation rate of the aluminum electrode was increased to 5 Å/s, aluminum nanoparticles will penetrate into the film of **TPA-BT** because of the rough surface and loose intermolecular packing of the film, as well as the greater momentum of aluminum nanoparticles. The penetrated aluminum nanoparticles will interact with **TPA-BT** molecules and enhance intramolecular or intermolecular charge transfer in the excited state, resulting in a stable charge transfer state[50-54]. When the device is powered off or under non-degrading reverse fields, the ON state of the memory device can still remain due to the stable localization of electrons in acceptor fragment. Therefore, the performance of the device is WORM behavior. When **TPA-BT** layer was covered with a layer of LiF, aluminum nanoparticles did not have enough energy to penetrate to the LiF layer and all of the aluminum nanoparticles were almost blocked outside of the LiF layer. So the device with the structure of ITO/**TPA-BT**/LiF/Al showed initial DRAM behavior. In contrast, aluminum nanoparticles may not easily penetrate into the film of **CZ-BT** due to the close intermolecular packing and more flat surface of the film, so the intramolecular or intermolecular CT of **CZ-BT** in film is hardly affected and still remain unstable. Therefore the device of **CZ-BT** still showed initial DRAM behavior.

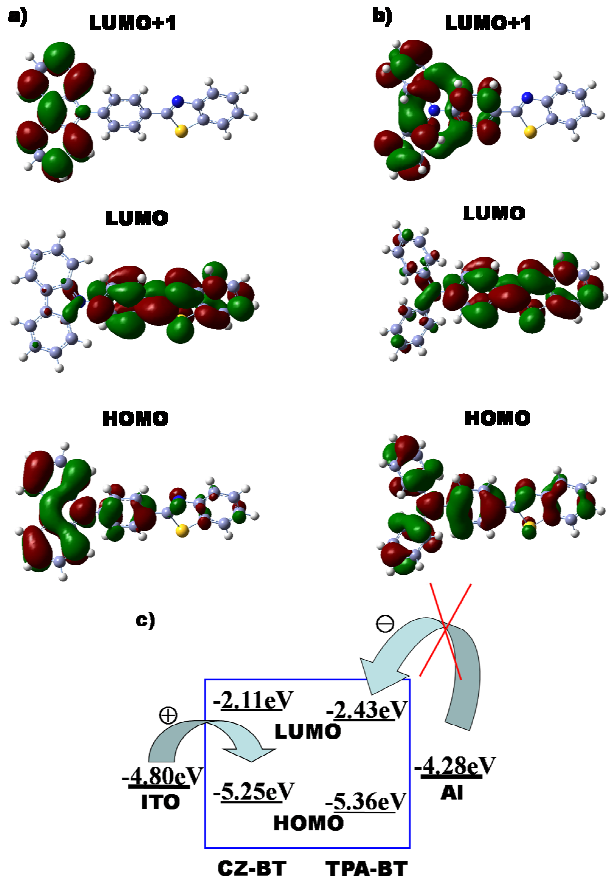

Fig. 6 LUMOs+1, LUMOs and HOMOs of (a) **CZ-BT** and (b) **TPA-BT**. (c) Energy level diagram for the ITO/compound/Al devices. The work functions of ITO and Al electrodes are -4.80 and -4.28 eV, respectively.

Conclusions

In summary, two small molecules containing the same electron-deficient moiety with different electron-rich moieties were synthesized and fabricated as the electroactive organic layers of the sandwich-structure memory devices. The devices based on the two compounds demonstrated DRAM memory storage performance because of the unstable CT states of the two compounds. But **CZ-BT** containing carbazole fragment stacked more closely and orderly in the thin film than **TPA-BT** during the vacuum-deposition, resulting in lower operating voltage, which are highly desirable for low-power consumption data-storage devices. In addition, the device based on **TPA-BT** exhibited WORM memory storage performance when the aluminum evaporation rate was increased to 5 Å/s. But the device based on **CZ-BT** still exhibited original DRAM behavior. Another conclusion is that the device based on **TPA-BT** exhibited initial DRAM type in the case of aluminum evaporation rate of 5 Å/s when a layer of LiF was added between **TPA-BT** film and ITO layer. The molecular structure, thin-film morphology, and the aluminum evaporation rate were identified to play vital roles in the electroactive layer and the devices performance will be better by enhancing the intermolecular interactions and orderly accumulation of molecules. We hope these results discussed here can provide a reference to the design and synthesis of electrical storage volatile material and stable memory device with low

power consumption.

Experimental section

Materials

Triphenylamine (95%), carbazole (CP), phosphorus oxychloride (95%), 2-aminothiophenol (95%), 4-bromobenzaldehyde (98%), 18-crown-6 (CP) and o-dichlorobenzene (98%) were purchased from TCI, Alfa Aesar, and Aladdin Co., Ltd, respectively. Other solvents and drugs were all purchased from Sinopharm reagent Co., Ltd and used as received without further purification.

Preparation of CZ-BT and TPA-BT

4-(9H-carbazol-9-yl)benzaldehyde (3). Carbazole **1** (5.21 g, 30 mmol), 4-bromobenzaldehyde (8.5 g, 45 mmol), anhydrous potassium carbonate (8.66 g, 0.135 mol), copper (4.77 g, 75 mmol), 18-crown-6 (1.19 g，4.5 mmol) were added together into 250 mL three-necked flask, then 150 mL o-dichlorobenzene was added to the above mixture. The mixture was heated to 180 ^{o}C and stirred under argon atmosphere for 48 hours. Then the mixture was cooled to room temperature and the o-dichlorobenzene was removed under reduced pressure. The yellow powdered solid was isolated after column chromatography (n-hexane/ehtyl acetate = 4 : 1). Yield: 70%. ^{1}H NMR (400 MHz, $CDCl_3$) δ (ppm): 10.12 (s, 1H), 8.16-8.13 (m, 4H), 7.80 (d, J = 8.30 Hz, 2H), 7.51 (d, J = 8.19 Hz, 2H), 7.44 (t, J = 7.62 Hz, 2H), 7.34 (t, J = 7.40 Hz, 2H).

2-(4-(9H-carbazol-9-yl)phenyl)benzo[d]thiazole (CZ-BT). Compound **3** (1.7 g, 6.27 mmol) and 2-aminothiophenol (0.788 g, 6.3 mmol) were added into DMSO and the mixture was heated to 150 ^{o}C and stirred for 6 h. The mixture was cooled to room temperature and poured into ice water, and then the mixture was filtered and washed with deionized water. The crude product was purified by silica gel chromatography with ethyl acetate-petroleum ether (volume ratio = 1 : 10) as the eluent to afford **CZ-BT** as white solid. Yield: 95%. ^{1}H NMR (400 MHz, d_6-DMSO) δ (ppm): 8.39 (s,2H), 8.27 (s, 2H), 8.21 (d, J = 8.03 Hz, 1H), 8.13 (d, J = 8.12 Hz, 1H), 7.88 (d, J = 8.53 Hz, 2H), 7.51 (d, J = 24.39 Hz, 6H), 7.34 (s, 2H). ^{13}C NMR (400 MHz, $CDCl_3$) δ(ppm): 166.52, 153.77, 139.96, 139.68, 134.74, 131.86, 128.62, 126.73, 126.11, 125.76, 125.00, 123.30, 122.94, 121.31, 120.03, 109.40. HRMS (ESI, m/z) calcd. for $C_{25}H_{16}N_2S$: 377.1112 ($M+H^+$). Found: 377.1107 ($M+H^+$).

4-(diphenylamino)benzaldehyde (4). DMF (8 mL) was added into 100 mL three-necked flask and stirred in an ice bath for 30 min, and then phosphorus oxychloride (4 mL) was added slowly into the mixture. After 1.5 h, the resulting viscous liquid was poured into a solution of triphenylamine **2** (4.9 g, 20 mmol) in chloroform (50 mL) at 80 ^{o}C and stirred for 7 h. The mixture was extracted repeatedly with chloroform. The organic layer was dried over anhydrous magnesium sulfate, the solvent was removed under reduced pressure. The crude product was purified through silica gel column with ethyl acetate and petroleum ether (volume ratio = 1 : 10). Yield: 85%. ^{1}H-NMR (400 MHz, d_6-DMSO) δ (ppm): 9.75 (s, 1H), 7.70 (d, J = 8.68 Hz, 2H), 7.40 (t, J = 7.72 Hz, 4H), 7.24-7.15 (m, 6H), 6.87 (d, J = 8.71 Hz, 2H).

4-(benzo[d]thiazol-2-yl)-N, N-diphenylaniline (TPA-BT). Compound **4** (1.01 g, 3.7 mmol), 2-aminothiophenol (0.488 g, 3.9 mmol) and DMSO (50 mL) were added to a single-necked flask. After stirring for 6 h at 160 ^{o}C, the reaction mixture was cooled to room temperature, then was poured into ice water and isolated by filtration. The final light yellow product was obtained by column chromatography with dichloromethane and petroleum ether (volume ratio = 1 : 3). Yield: 90%. ^{1}H NMR (400 MHz, d_6-DMSO) δ (ppm): 8.09 (d, J = 7.99 Hz, 1H), 7.98 (dd, J = 8.46, 12.64 Hz, 3H), 7.50 (d, J = 8.03 Hz, 1H), 7.40 (dd, J = 7.48, 15.43 Hz, 5H), 7.17 (dd, J = 7.68, 11.00 Hz, 6H), 7.01 (d, J = 8.69 Hz, 2H). ^{13}C NMR (400 MHz, $CDCl_3$) δ(ppm): 167.71, 154.18, 150.30, 146.79, 134.71, 129.43, 128.46, 126.44, 126.10, 125.31, 124.63, 123.95, 122.67, 121.62, 121.41. HRMS (ESI, m/z) calcd. for $C_{25}H_{18}N_2S$: 379.1269 ($M+H^+$). Found: 379.1267 ($M+H^+$).

Fabrication of the memory device

The indium tin oxide (ITO) glass substrate was carefully pre-cleaned sequentially with deionized water, acetone and alcohol by ultrasonic bath for 30 minutes, respectively. The electroactive organic film was deposited under high vacuum (10^{-6} Torr). The film thickness was about 200 nm. An aluminum (Al) layer with thickness of about 100 nm was thermally evaporated and deposited onto the organic surface at about 2×10^{-6} Torr with the rate range from 0 to 5 Å/s through a shadow mask to form the top electrode. An active device area of 0.0314 mm^2 was obtained. In addition, the LiF layer with thickness of about 5 nm was formed with the rate of 2 Å/s under the same other conditions. The devices with the structures of ITO/organic compound/Al and ITO/organic compound/LiF/Al were obtained.

Measurement

^{1}H NMR spectra were obtained on Inova 400 MHz FT-NMR spectrometers. Thermogravimetric analysis (TGA) was conducted on a TA Instruments Dynamic TGA 2950 at a heating rate of 10 ^{o}C·min^{-1} under an N_2 flow rate of 50 mL·min^{-1}. UV-vis absorption spectra were recorded by a PerkinElmer Lambda-17 spectrophotometer in the 250-700nm spectral region at room temperature. Cyclic voltammetry was performed at room temperature using a platinum-carbon working electrode, a reference electrode Ag/AgCl, and a counter electrode (Pt wire) at a sweep rate of 100 mV·s^{-1} on a Corr-Test CS Electrochemical Workstation analyzer, a 0.1 M solution of tetrabutylammonium perchlorate (TBAP) in anhydrous dichloromethane was used. Scanning electron microscopy (SEM) images were taken on a Hitachi S-4700 scanning electron microscope. Atomic force microscopy (AFM) measurements were performed by using a MFP-3DTM (Digital Instruments/Asylum Research) AFM instrument to measure the surface morphology of films. X-ray diffraction (XRD) patterns were taken on an X'Pert-Pro MPD X-ray diffractometer. All electrical measurements of the devices were characterized under ambient conditions without any encapsulation using an Agilent Technologies B1500A Semiconductor device Analyzer equipped with a TTPX low and variable temperature probe station.

Acknowledgements

This work was financially supported by the Chinese Natural Science Foundation (21176164, 21206102 and 21336005), NSF of Jiangsu Province (BE2013052), a project of the Department of Education of Jiangsu Province (12KJB430011), Suzhou Nano-project (ZXG2012023) and Project supported by the Specialized Research Fund for the Doctoral Program of Higher Education of China (Grant No. 20113201130003 and 20123201120005).

Notes and references

[a] College of Chemistry, Chemical Engineering and Materials Science, Collaborative Innovation Center of Suzhou Nano Science and Technology, Soochow University, Suzhou, Jiangsu 215123, China. Fax: +86 512 65880367; Tel: +86 512 65880368; E-mail: lihuaw@suda.edu.cn; lujm@suda.edu.cn.
[b] State Key Laboratory of Treatments and Recycling for Organic Effluents by Adsorption in Petroleum and Chemical Industry, Suzhou 215123, China.

Electronic Supplementary Information (ESI) available: [TGA, 3D AFM images, Stimulus effect of read cycles, I-V characteristic]. See DOI: 10.1039/b000000x/

1 Q. D. Ling, F. C. Chang, Y. Song, C. X. Zhu, D. J. Liaw, D. S. H. Chan, E. T. Kang and K. G. Neoh, *J. Am. Chem. Soc.*, 2006, **128**, 8732.
2 Y. Yang, J. Ouyang, L. Ma, R. J. H. Tseng and C. W. Chu, *Adv. Funct. Mater.*, 2006, **16**, 1001.
3 B. Cho, S. Song, Y. Ji, T. W. Kim and T. Lee, *Adv. Funct. Mater.*, 2011, **21**, 2806.
4 Q. D. Ling, D. J. Liaw, C. Zhu, D. S. H. Chan, E. T. Kang and K. G. Neoh, *Prog. Polym. Sci.*, 2008, **33**, 917.
5 Y. H. Chou, W. Y. Lee and W. C. Chen, *Adv. Funct. Mater.*, 2012, **22**, 4352.
6 J. Liu, Z. Yin, X. Cao, F. Zhao, L. Wang, W. Huang and H. Zhang, *Adv. Mater.*, 2013, **25**, 233.
7 J. Liu, Z. Zeng, X. Cao, G. Lu, L. H. Wang, Q. L. Fan, W. Huang and H. Zhang, *Small*, 2012, **8**, 3517.
8 J. Lee, E. Lee, S. Kim, G. S. Bang, D. A. Shultz, R. D. Schmidt, M. D. E. Forbes and H. Lee, *Angew. Chem., Int. Ed.*, 2011, **50**, 4414.
9 A. D. Yu, T. Kurosawa, Y. C. Lai, T. Higashihara, M. Ueda, C. L. Liu and W. C. Chen, *J. Mater. Chem.*, 2012, **22**, 20754.
10 Y. W. Lin, C. J. Lin, Y. H. Chou, C. L. Liu, H. C. Chan and W. C. Chen, *J. Mater. Chem. C*, 2013, **1**, 5336.
11 S. J. Liu, W. P. Lin, M. D. Yi, W. J. Xu, C. Tang, Q. Zhao, S. H. Ye, X. M. Liu and W. Huang, *J. Mater. Chem.*, 2012, **22**, 22964.
12 P. Wang, S. J. Liu, Z. H. Lin, X. C. Dong, Q. Zhao, W. P. Lin, M. D. Yi, S. H. Ye, C. X. Zhu and W. Huang, *J. Mater. Chem.*, 2012, **22**, 9576.
13 S. J. Liu, P. Wang, Q. Zhao, H. Y. Yang, J. I. Wong, H. B. Sun, X. C. Dong, W. P. Lin and W. Huang, *Adv. Mater.*, 2012, **24**, 2901.
14 W. P. Lin, S. J. Liu, T. Gong, Q. Zhao and W. Huang, *Adv. Mater.*, 2014, **26**, 570.
15 S. J. Liu, Z. H. Lin, Q. Zhao, Y. Ma, H. F. Shi, M. D. Yi, Q. D. Ling, Q. L. Fan, C. X. Zhu, E. T. Kang and W. Huang, *Adv. Funct. Mater.*, 2011, **21**, 979.
16 D. I. Son, T. W. Kim, J. H. Shim, J. H. Jung, D. U. Lee, J. M. Lee, W. I. Park and W. K. Choi, *Nano Lett.*, 2010, **10**, 2441.
17 J. Lee, H. Chang, S. Kim, G. S. Bang and H. Lee, *Angew. Chem., Int. Ed.*, 2009, **48**, 8501.
18 X. D. Zhuang, Y. Chen, G. Liu, P. P. Li, C. X. Zhu, E. T. Kang, K. G. Noeh, B. Zhang, J. H. Zhu and Y. X. Li, *Adv. Mater.*, 2010, **22**, 1731.
19 T. W. Kim, H. Choi, S. H. Oh, G. Wang, D. Y. Kim, H. Hwang and T. Lee, *Adv. Mater.*, 2009, **21**, 2497.
20 N. H. You, C. C. Chueh, C. L. Liu, M. Ueda and W. C. Chen, *Macromolecules*, 2009, **42**, 4456.
21 S. L. Lim, Q. Ling, E. Y. H. Teo, C. X. Zhu, D. S. H. Chan, E. T. Kang and K. G. Neoh, *Chem. Mater.*, 2007, **19**, 5148.
22 W. Kwon, B. Ahn, D. M. Kim, Y. G. Ko, S. G. Hahm, Y. Kim, H. Kim and M. Ree, *J. Phys. Chem. C*, 2011, **115**, 19355.
23 B. Ahn, D. M. Kim, J. C. Hsu, Y. G. Ko, T. J. Shin, J. Kim, W. C. Chen and M. Ree, *Macro. Lett.*, 2013, **2**, 555.
24 Y. G. Ko, W. Kwon, H. J. Yen, C. W. Chang, D. M. Kim, K. Kim, S. G. Hahm, T. J. Lee, G. S. Liou and M. Ree, *Macromolecules*, 2012, **45**, 3749.
25 S. L. Lian, C. L. Liu and W. C. Chen, *Appl. Mater. Interfaces*, 2011, **3**, 4504.
26 Y. K. Fang, C. L. Liu and W. C. Chen, *J. Mater. Chem.*, 2011, **21**, 4778.
27 H. C. Wu, C. L. Liu and W. C. Chen, *Polym. Chem.*, 2013, **4**, 5261.
28 S. F. Miao, H. Li, Q. F. Xu, N. J. Li, J. W. Zheng, R. Sun, J. M. Lu and C. M. Li, *J. Mater. Chem.*, 2012, **22**, 16582.
29 W. S. Ren, Y. X. Zhu, J. F. Ge, X. F. Xu, R. Sun, N. J. Li, H. Li, Q. F. Xu, J. W. Zheng and J. M. Lu, *Phys. Chem. Chem. Phys.*, 2013, **15**, 9212.
30 Y. H. Zhang, H. Zhuang, Y. Yang, X. F. Xu, Q. Bao, N. J. Li, H. Li, Q. F. Xu, J. M. Lu and L. H. Wang, *J. Phys. Chem. C*, 2012, **116**, 22832.
31 S. F. Miao, H. Li, Q. F. Xu, Y. Y. Li, S. J. Ji, N. J. Li, L. H. Wang, J. W. Zheng and J. M. Lu, *Adv. Mater.*, 2012, **24**, 6210.
32 H. Zhuang, Q. J. Zhang, Y. X. Zhu, X. F. Xu, H. F. Liu, N. J. Li, Q. F. Xu, H. Li, J. M. Lu and L. H. Wang, *J. Mater. Chem. C*, 2013, **1**, 3816.
33 K. Kim, Y. K. Fang, W. Kwon, S. Pyo, W. C. Chen and M. Ree, *J. Mater. Chem. C*, 2013, **1**, 4858.
34 S. Park, T. J. Lee, D. M. Kim, J. C. Kim, K. Kim, W. Kwon, Y. G. K. H. Choi, T. Chang and M. Ree, *J. Phys. Chem. B*, 2010, **114**, 10294.
35 D. M. Kim, S. Park, T. J. Lee, S. G. Hahm, K. Kim, J. C. Kim, W. Kwon and M. Ree, *Langmuir*, 2009, **25**, 11713.
36 S. G. Hahm, T. J. Lee, D. M. Kim, W. Kwon, Y. G. Ko, T. Michinobu and M. Ree, *J. Phys. Chem. C*, 2011, **115**, 21954.
37 D. C. Wei, B. Wu, Y. L. Guo, G. Yu and Y. Q. Liu, *Acc. Chem. Res.*, 2013, **46**, 106.
38 B. X. Mi, Y. Q. Dong, Z. Li, J. W. Y. Lam, M. Häußler, H. H. Y. Sung, H. S. Kwok, Y. Dong, I. D. Williams, Y. Q. Liu, Y. Luo, Z. G. Shuai, D. B. Zhu and B. Z. Tang, *Chem. Commun.*, 2005, **28**, 3583.
39 Q. D. Ling, E. T. Kang, K. G. Neoh, Y. Chen, X. D. Zhuang, C. X. Zhu and D. S. H. Chan, *Appl. Phys. Lett.*, 2008, **92**, 143302.
40 X. D. Zhuang, Y. Chen, B. X. Li, D. G. Ma, B. Zhang and Y. Li, *Chem. Mater.*, 2010, **22**, 4455.
41 K. Uchida, E. Tsuchida, Y. Aoi, S. Nakamura and M. Irie, *Chem. Lett.*, 1999, **28**, 63.
42 C. Y. Huang, G. Q. Jiang and R. Advincula, *Macromolecules*, 2008, **41**, 4661.
43 D. J. Liaw, K. L. Wang and F. C. Chang, *Macromolecules*, 2007, **40**, 3568.
44 Y. L. Liu, Q. D. Ling, E. T. Kang, K. G. Neoh, D. J. Liaw, K. L. Wang, W. T. Liou, C. X. Zhu and D. S. H. Chan, *J. Appl. Phys.*, 2009, **105**, 044501.

45 M. Gsänger, J. H. Oh, M. Könemann, H. W. Höffken, A. M. Krause, Z. Bao and F. Wurthner, *Angew. Chem., Int. Ed.*, 2010, **49**, 740.
46 H. Li, N. J. Li, H. W. Gu, Q. F. Xu, F. Yan, J. M. Lu, X. W. Xia, J. F. Ge and L. H. Wang, *J. Phys. Chem. C*, 2010, **114**, 6117.
47 C. L. Liu, T. Kurosawa, A. D. Yu, T. Higashihara, M. Ueda and W. C. Chen, *J. Phys. Chem. C*, 2011, **115**, 5930.
48 T. Kurosawa, Y. C. Lai, T. Higashihara, M. Ueda, C. L. Liu and W. C. Chen, *Macromolecules*, 2012, **45**, 4556.
49 P. Cias, C. Slugovc and G. Gescheidt, *J. Phys. Chem. A*, 2011, **115**, 14519.
50 J. Y. Ouyang, C. W. Chu, C. R. Szmanda, L. P. Ma and Y. Yang, *nature materials*, 2004, **3**, 918.
51 A. Prakash and J. Y. Ouyang, J. L. Lin, Y. Yang, *J. Appl. Phys.*, 2006, **100**, 054309-1.
52 L. Wang, E. K. Wang, *Electrochemistry Communications*, 2004, **6**, 49.
53 Z. H. Sun, C. X. Wang, J. X. Yang, B. Zhao and J. R. Lombardi, *J. Phys. Chem. C*, 2008, **112**, 6093.
54 R. J. Tseng, C. O. Baker, B. Shedd, J. X. Huang, R. B. Kaner, J. Y. Ouyang and Y. Yang, *Appl. Phys. Lett*., 2007, 90, 053101-1.